Available online at www.sciencedirect.com
SCIENCE DIRECT®
Marine Pollution Bulletin 49 (2004) 1013–1024
MARINE POLLUTION BULLETIN
www.elsevier.com/locate/marpolbul

Coastal pollution hazards in southern California observed by SAR imagery: stormwater plumes, wastewater plumes, and natural hydrocarbon seeps

Paul M. DiGiacomo [a,*], Libe Washburn [b], Benjamin Holt [a], Burton H. Jones [c]

[a] Jet Propulsion Laboratory, California Institute of Technology, MS 300-323, 4800 Oak Grove Drive, Pasadena, CA 91109-8001, USA
[b] Department of Geography, Institute for Computational Earth System Science, University of California, Santa Barbara, CA 93106-3060, USA
[c] Hancock Institute for Marine Studies, University of Southern California, University Park, Los Angeles, CA 90089-0371, USA

Abstract

Stormwater runoff plumes, municipal wastewater plumes, and natural hydrocarbon seeps are important pollution hazards for the heavily populated Southern California Bight (SCB). Due to their small size, dynamic and episodic nature, these hazards are difficult to sample adequately using traditional in situ oceanographic methods. Complex coastal circulation and persistent cloud cover can further complicate detection and monitoring of these hazards. We use imagery from space-borne synthetic aperture radar (SAR), complemented by field measurements, to examine these hazards in the SCB. The hazards are detectable in SAR imagery because they deposit surfactants on the sea surface, smoothing capillary and small gravity waves to produce areas of reduced backscatter compared with the surrounding ocean. We suggest that high-resolution SAR, which obtains useful data regardless of darkness or cloud cover, could be an important observational tool for assessment and monitoring of coastal marine pollution hazards in the SCB and other urbanized coastal regions.

Keywords: Hydrocarbon seeps; Runoff; Slicks; Southern California; Synthetic aperture radar; Wastewater, plumes

1. Introduction

The rapidly expanding southern California megalopolis, which includes the coastal counties of San Diego, Orange, Los Angeles, Ventura and Santa Barbara, is home to approximately 20 million people who represent nearly 25% of the total US coastal population (Culliton et al., 1990). Activities of this large human population result in the discharge of a broad range of pollutants into coastal waters of the Southern California Bight (SCB; Fig. 1) including pesticides, fertilizers, trace metals, synthetic organic compounds, petroleum, and pathogens (National Research Council, 1990, 1993). These pollutants enter coastal waters through two main pathways: stormwater runoff from heavily urbanized watersheds and wastewater discharge from publicly owned treatment works (POTWs) and shoreline industries. Additionally, an important pathway for hydrocarbon pollutants to enter waters of the SCB is natural hydrocarbon seepage from coastal sources on the sea floor from Los Angeles to Point Conception, CA. Southern California has a complex physical circulation due to varying bathymetry, offshore islands, and numerous prominent headlands (Hickey, 1992; DiGiacomo and Holt, 2001), which likely affect the transport of these pollution hazards.

Urban stormwater runoff is currently the most significant pollution hazard for coastal waters in the SCB. Stormwater runoff rates and volumes are growing in

* Corresponding author. Tel.: +1 818 354 8189; fax: +1 818 393 6720.
E-mail address: pmd@pacific.jpl.nasa.gov (P.M. DiGiacomo).

0025-326X/$ - see front matter © 2004 Elsevier Ltd. All rights reserved.
doi:10.1016/j.marpolbul.2004.07.016

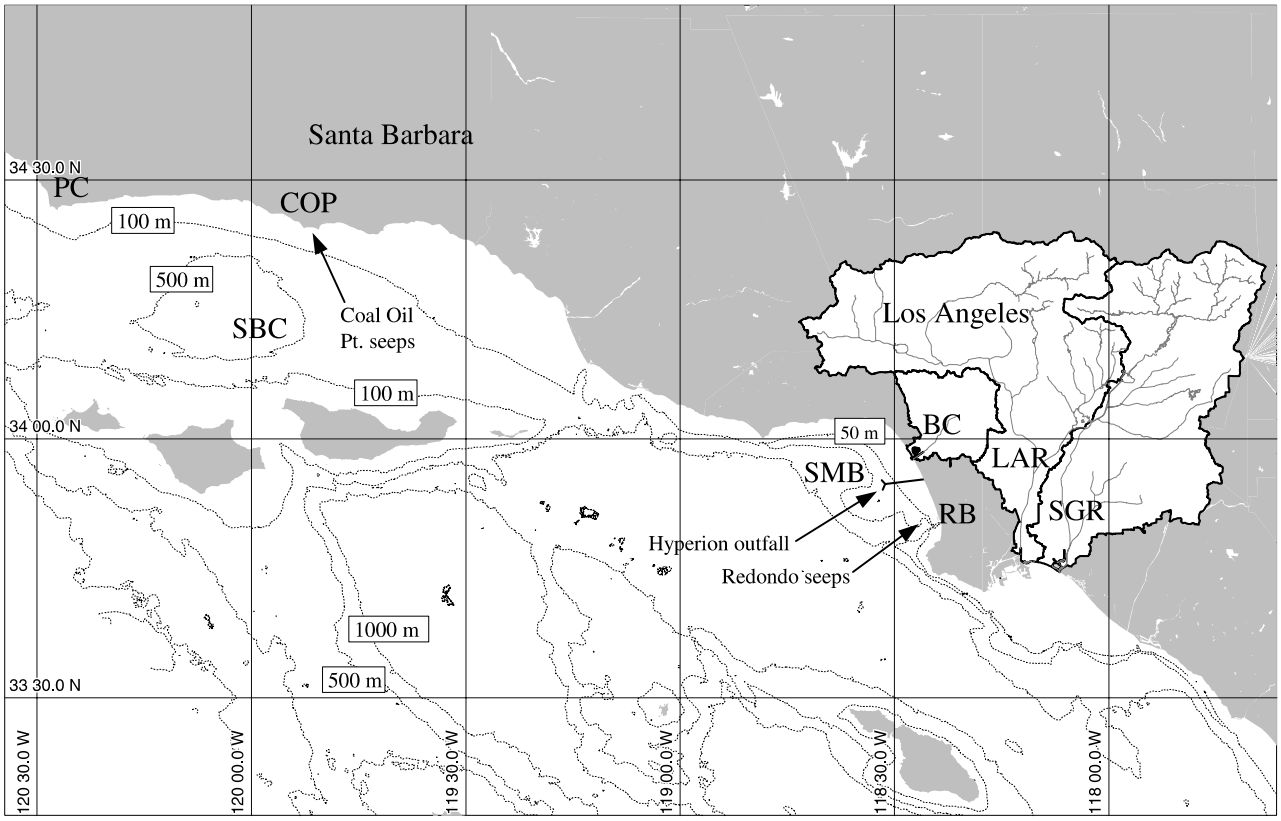

Fig. 1. Map of the northern part of the Southern California Bight showing study locations of pollutant types examined in this study. Watersheds for the Los Angeles River (LAR), San Gabriel River (SGR), and Ballona Creek (BC) are outlined in bold. Point Conception (PC), Santa Barbara Channel (SBC), Coal Oil Point (COP), Santa Monica Bay (SMB), and Redondo Beach (RB) are also identified.

urban regions such as Los Angeles due to the increasing population and proliferation of impervious surfaces (Schiff et al., 2000). Increases in the number of sources, types of constituents, and concentrations of pollutants in stormwater runoff accompany the rising population of this region (Dailey et al., 1993). Episodic storm events, typically occurring late fall through early spring, contribute more than 95% of the annual runoff volume and pollutant load in the SCB (Schiff et al., 2000). These inputs modify the physical and biogeochemical state of coastal waters. Stormwater runoff changes density stratification and coastal circulation processes, nutrient distributions, suspended sediment concentrations, phytoplankton biomass, and primary productivity (National Research Council, 1993). A recent study in Santa Monica Bay (SMB), CA found that runoff plumes from single rainfall events of ~2 cm total precipitation have cross-shelf length scales of 4–7 km, alongshore scales of at least 10 km, and vertical scales of about 10 m (Washburn et al., 2003). Elevated nutrient concentrations in stormwater runoff in SMB promote rapid phytoplankton growth yielding chlorophyll concentrations in excess of 20 mg m^{-3} (Jones et al., 2002), a result suggesting that stormwater runoff might increase the incidence of harmful algal blooms. Urban stormwater runoff is also a hazard to human health (Noble et al., 2003). For example, an epidemiological study reported by Haile et al. (1996, 1999) and Wang (1997) found that a broad range of adverse symptoms occurred in ocean swimmers exposed to recent stormwater runoff near storm drains in SMB. Stormwater runoff plumes also exhibit toxicity when freshwater concentrations of the plumes are high (Bay et al., 1999).

Wastewater discharge from POTWs is also a significant marine pollution hazard in the SCB. Cumulatively POTWs discharge approximately 3.9×10^6 m^3 day^{-1} (1.03×10^9 gal day^{-1}) of treated wastewater effluent into southern California coastal waters (Schiff et al., 2000). About half of this effluent receives secondary treatment. Discharge of the effluent offshore at depth (typically ~60 m) and subsequent formation of submerged wastewater plumes promote dilution and dispersal of contaminant loadings (Fischer et al., 1979). Occasionally, however, the submerged plumes surface (Jones et al., 1990; Dalkey and Shisko, 1996), leading to possible onshore transport of contaminants by local atmospheric and oceanographic processes.

Another significant pollution hazard in southern California is natural hydrocarbon seepage. Hydrocarbon seeps in the Santa Barbara Channel, and to a

much lesser extent in SMB (Fig. 1), deposit tar and oil over many southern California beaches (Hartman and Hammond, 1981). Furthermore, gaseous hydrocarbon emissions from the seeps contribute significantly to atmospheric pollution in the form of reactive organic gases for Santa Barbara and Ventura counties (Killus and Moore, 1991; Hornafius et al., 1999; Quigley et al., 1999).

Key to evaluating and managing pollution hazards posed by stormwater runoff, surfacing wastewater plumes, and hydrocarbon seepage is the acquisition of accurate, timely data at the relevant scales of space and time. Acquiring this data can be challenging using either in situ or remote sensing approaches because these pollution hazards are typically episodic or ephemeral features with limited spatial extents. Ship-based sampling, for example, is very slow and expensive, requires extensive advance planning, and is difficult to conduct in poor weather. The impracticality of obtaining long time series from shipboard sampling limits observation of transient pollution events. Moorings, on the other hand, are well suited to single point time series measurements, but their initial expense, maintenance, and vulnerability generally limit them to spatially sparse arrays. Satellite remote sensing, particularly those sensors using visible, near- and thermal infrared portions of the electromagnetic spectrum, is valuable in the coastal regions since it can provide daily, synoptic time-series data. However, these sensors have only moderate ground resolution (e.g., 0.3–1 km) and viewing is frequently limited by cloud cover. Active microwave remote sensing approaches overcome some of these limitations.

A valuable, but still under-used active remote sensing approach for coastal water quality applications, is satellite-borne synthetic aperture radar (SAR) (e.g., Holt, 2004). SAR imagery provides high-resolution ($\leqslant$100 m ground resolution) active microwave observations of sea-surface roughness that are independent of weather and availability of light. Factors modulating surface roughness include wind, interactions of waves and currents, and the presence of surfactants on the ocean surface. Observed surface roughness variability can distinguish surface manifestations of the three pollution hazards described above from the ambient ocean because they all contain surfactants. The surfactants smooth capillary and small gravity waves, which reduces surface roughness and thus radar backscatter. The smoothed surfactant-covered areas appear darker on SAR imagery compared with the usually wind-roughened surrounding ocean, which has higher backscatter and thus appears brighter on SAR imagery. SAR imagery also visualizes complex, small-scale oceanographic processes, such as coastal eddies (e.g., Munk et al., 2000; DiGiacomo and Holt, 2001), which are likely important in controlling the transport, near shore residence times, and fates of pollutants associated with these hazards. SAR imagery has been used to identify significant, and often illegal, discharges from ships (e.g., Gade and Alpers, 1999; Lu, 2003; Pavlakis et al., 2001), to examine natural seeps in the Gulf of Mexico (De Beukelaer et al., 2003), and to observe stormwater and sewage runoff in southern California (Svejkovsky and Jones, 2001). SAR has also been used for monitoring oil spills from ships and platforms (e.g., Fingas and Brown, 1997; Espedal and Johannessen, 2000; Jones, 2001).

The ability of SAR to detect pollution hazards is limited by environmental conditions, particularly wind and waves (Gade et al., 1998; Trivero et al., 1998; DiGiacomo and Holt, 2001; Svejkovsky and Jones, 2001). Successful imaging of oil slicks using SAR requires that surface wind speeds fall in a fairly narrow range. At very low wind speeds (less than 2–3 m s^{-1}), little microwave energy transmitted to the sea surface is backscattered toward the SAR, resulting in dark areas, broadly distributed over a SAR image. Under these conditions oil slicks cannot be differentiated from smooth ambient waters. At high wind speeds increased surface roughness results in dispersal and mixing of the oil into the upper ocean. Petrogenic hydrocarbons may be detectable on SAR imagery until winds exceed 10–14 m s^{-1}, depending on sea state and heaviness of oil (e.g., Espedal et al., 1998; Espedal et al., 1999; Wismann et al., 1998). Biogenic oils (e.g., phytoplankton exudates) are generally not detectable when winds exceed 7–8 m s^{-1} (DiGiacomo and Holt, 2001).

Sorting out ambiguous surface slick signatures is an area of active research, requiring repeat imaging, analysis of wind time series, and knowledge of sources (Espedal and Wahl, 1999; Solberg et al., 1999). Perhaps the most significant constraint on the routine use of SAR for coastal pollution monitoring is the inconsistent temporal coverage afforded by all SAR platforms to date. From a single sensor, with swath widths from 100–500 km, SAR observation frequency is variable, ranging from a best of twice-per-day to several observations per week.

The purpose of this study is to evaluate SAR as a tool for observing three common pollution hazards off the coast of southern California: stormwater runoff, wastewater plumes, and natural hydrocarbon seepage. We provide an analysis of regional SAR imagery supported by comparisons with other data sources including shore-based high frequency (HF) radar and in situ measurements. Our results suggest that SAR, particularly in combination with HF radar, could provide valuable information about these pollution hazards in support of improved coastal management in the SCB and in other urbanized coastal regions. Improved access to SAR data is also needed, as well as studies linking SAR data with in situ water quality indicators. Together

these data may allow synoptic assessments of the consequences for human health and ecological impacts of these pollution hazards.

2. Methods

2.1. SAR data and imaging characteristics

The ERS-1 and ERS-2 SAR data (12.5 m pixel size) were obtained from the European Space Agency (ESA); images were acquired at the receiving station operated by the Canada Centre of Remote Sensing in Prince Albert, Saskatchewan. Both platforms have the same C-band (5.3 GHz) SAR instrument, which operates at a polarization of vertical transmit-vertical receive (VV) with a swath width of 100 km obtained over a fixed range of incidence angles from 20–26°. The nominal ERS-1 and ERS-2 orbits have 35-day repeat cycles and all data used were obtained during the descending (southward) portion of the sun-synchronous orbit at midmorning local time (~1830 UTC). This time of day generally precedes the afternoon sea breeze that is characteristic of the SCB (Dorman, 1982).

The Canadian Space Agency's RADARSAT SAR data were received by the same Prince Albert receiving station and processed at the Alaska Satellite Facility, located at the University of Alaska in Fairbanks, Alaska. Data were also acquired via an onboard tape recorder. The RADARSAT SAR operates at the same C-band frequency of 5.3 GHz as ERS, but at a polarization of horizontal transmit-horizontal receive (HH), which generally has lower ocean backscatter than VV for any given sea state and wind speed (e.g., Holt, 2004). Data were obtained in one of two configuration modes: (1) standard beam which has a swath width of 100 km, a pixel size of 12.5 m, and operates over varying fixed ranges of incidence angles; and (2) so-called ScanSAR Wide-beam B mode, which has a swath width of 450 km over incidence angles from 20–47° and a 100 m pixel size in the imagery presented here. RADARSAT has a 24-day repeat cycle in a sun-synchronous orbit with nominal 0600 or 1800 local times of acquisition.

2.2. In situ data

A number of existing field measurements were obtained to help interpret these SAR data. Daily precipitation data for downtown Los Angeles (Station 716) were acquired from the Los Angeles Department of Public Works (LADPW; http://www.ladpw.org), as were discharge data at 15-min intervals for Ballona Creek (Station F-38C) and the Los Angeles River (Station F319-R). Also obtained were hydrographic measurements made in SMB by the Environmental Monitoring Division of the City of Los Angeles's Bureau of Sanitation for monitoring sewage effluent from the Hyperion Wastewater Treatment Plant. These observations were carried out weekly from September 1987 through June 1994 and monthly thereafter until December 1997. Profiles of temperature, salinity, dissolved oxygen, and beam attenuation coefficient (660 nm wavelength), hereafter called beam C, were made using a CTD system and a beam transmissometer; for further details see Dalkey and Shisko (1996). Sea-surface observations (e.g., wind speed and direction) were available from NOAA buoys located in SMB off Redondo Beach (NDBC 46045) and near the middle of the Santa Barbara Channel (NDBC 46053).

2.3. High frequency radar data

Surface currents were measured hourly in the Santa Barbara Channel from two HF radars, one at Coal Oil Point (location indicated by triangle, Fig. 5C) and the other to the west near Refugio Beach. The radars operated at ~12 MHz and were configured to have a range of 42 km with a range resolution of 1.5 km and angular resolution of 5°. Surface current vectors are spatial averages over circles with radii of 3 km, which have been interpolated onto a 2 km square grid using the method described by Gurgel (1994). Additional details on the HF radars used in this analysis and their performance are given by Emery et al. (2004).

3. Results

3.1. Stormwater runoff plumes

SAR imagery of the Ballona Creek stormwater runoff discharge in Santa Monica Bay and coincident discharge and precipitation time series for two storm events are shown in Fig. 2. Ballona Creek accounts for about one third of the total stormwater runoff discharged annually into SMB (unpublished data, Los Angeles County Department of Public Works). The 8 November 1998 SAR data (Fig. 2A) reveals a stormwater plume imaged near the discharge peak. High surfactant loadings reduce backscatter in the stormwater plume (dark ocean areas, Fig. 2A) by ~10 dB relative to surrounding ocean waters (inset, Fig. 2A). The areal extent of this two-lobed feature - the breakwater at the mouth of Ballona Creek splits the discharge - is approximately 7 km^2. The feature extends offshore nearly 3 km, comparable to the offshore extent derived from shipboard measurements of the Ballona Creek plume in 1996 (Washburn et al., 2003). Cumulative event discharge volume from Ballona Creek up to the time of SAR image acquisition is 1.6×10^6 m^3 (Fig. 2B). This is associated with a cumulative event precipitation total of ~1.2 cm. Discharge averaged over 15 min intervals peaks at 152 $m^3 s^{-1}$ about

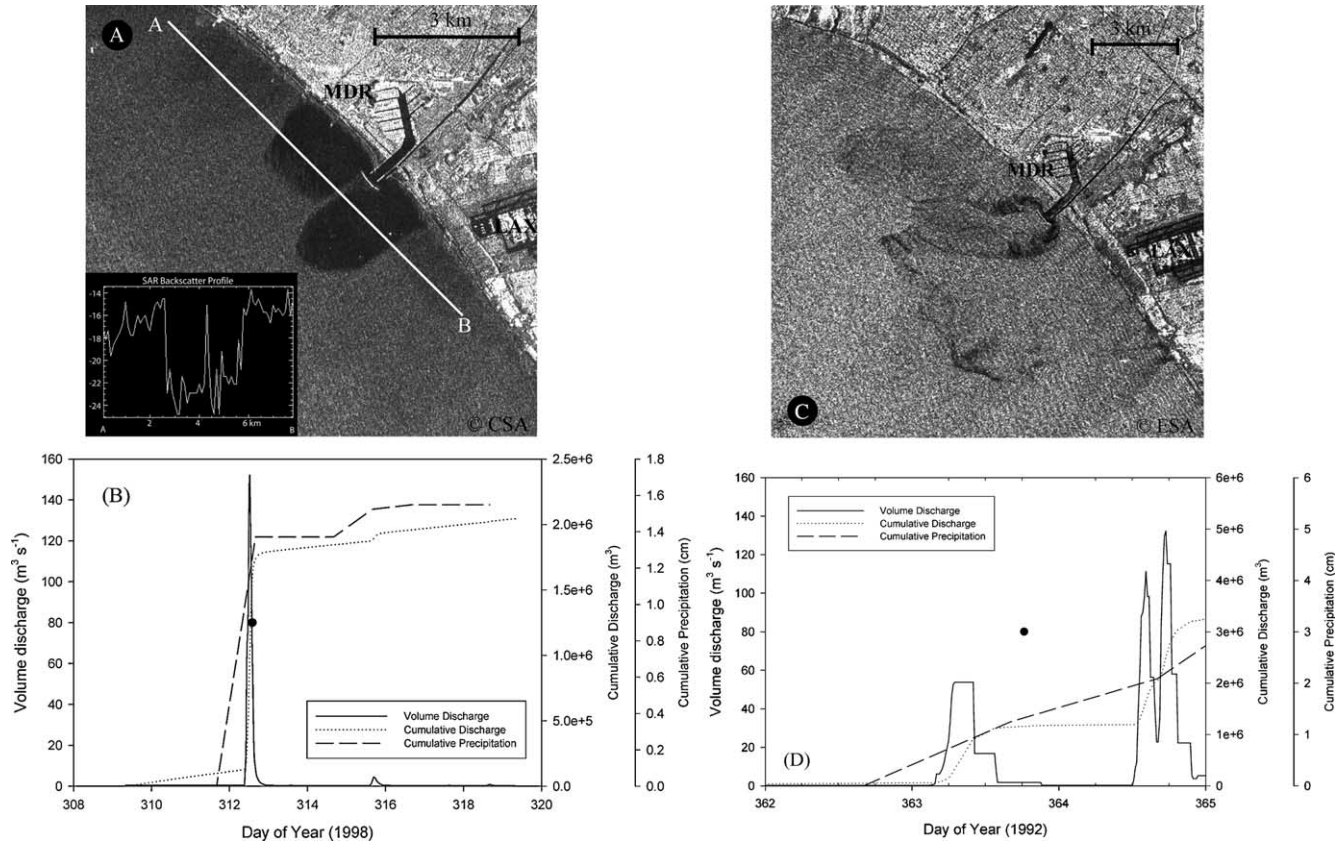

Fig. 2. SAR imagery of stormwater plumes from Ballona Creek, located just south of the entrance to Marina del Rey (MDR), California, at two stages in stormwater plume evolution. (A) RADARSAT-1 SAR image on 8 November 1998 at 1400 GMT (12.5 m pixels). Line AB marks location of SAR backscatter profile (inset). Los Angeles Airport (LAX) is also indicated. (B) Time series for Ballona Creek of volume discharge rate (solid line), cumulative discharge volume (dotted line), and cumulative precipitation (dashed line). Dot shows time of SAR image of panel (A). (C) As in panel (A) but ERS-1 SAR image from 28 December 1992 at 1834 GMT (12.5 m pixels). (D) As in panel B), but dot shows time of SAR image of panel (C).

1.5 h prior to image acquisition. A smaller discharge event observed for the same region on 28 December 1992 also exhibited a two-lobed feature, but had a much smaller area (~0.6 km^2, Fig. 2C). In this case the SAR image was acquired about 11 h after the discharge peak (Fig. 2D). There is also evidence of a decaying plume signature farther offshore, possibly resulting from the earlier timing of peak flow. Cumulative event discharge from Ballona Creek up to the time of SAR image acquisition was 1.1×10^6 m^3, about two thirds of the discharge observed in the 8 November 1998 event. The cumulative event precipitation total of ~1.3 cm was similar to the 8 November 1998 event, but the instantaneous volume discharge peaked at only 54 $m^3 s^{-1}$.

SAR imagery capturing stormwater runoff from the Los Angeles (LA) River into the Los Angeles-Long Beach (LA-LB) harbor area is presented in Fig. 3. Imagery from 28 December 1992 (Fig. 3A; same satellite acquisition pass as Fig. 2C) shows a runoff plume (dark region of reduced backscatter) from the LA River covering the central part of the harbor just offshore of the river mouth. The peak flow of the LA River, about 193 $m^3 s^{-1}$, occurred about 7.5 h before image acquisition (Fig. 3B). Cumulative event discharge from the LA River up to the time of image acquisition was 5.1×10^6 m^3, associated with a cumulative event precipitation total of ~1.3 cm. A plume from the San Gabriel River is also present in this image spreading westward along the offshore (southern) side of the LA-LB Harbor breakwater. Another plume from the LA River, observed in a 14 February 1995 SAR image (Fig. 3C), was significantly larger than the plume observed on 28 December 1992 (Fig. 3A). The 14 February 1995 image was acquired near the peak of the runoff event (Fig. 3D), and the stormwater plume from the LA River fills the eastern half of the harbor region, constrained only by the offshore breakwater (Fig. 3C). The cumulative event discharge volume from the LA River is 14.6×10^6 m^3 up to the time of the image of Fig. 3C and is associated with a cumulative event precipitation total of ~2.3 cm. The volume discharge peaked at 980 $m^3 s^{-1}$ at 1.75 h prior to image acquisition (Fig. 3D). In contrast to the previous open-coast observations (Fig. 2), this LA-LB harbor SAR imagery demonstrates that surfactants can rapidly cover most or all of a confined area following even small to moderate rainfall events. Partial coverage of the

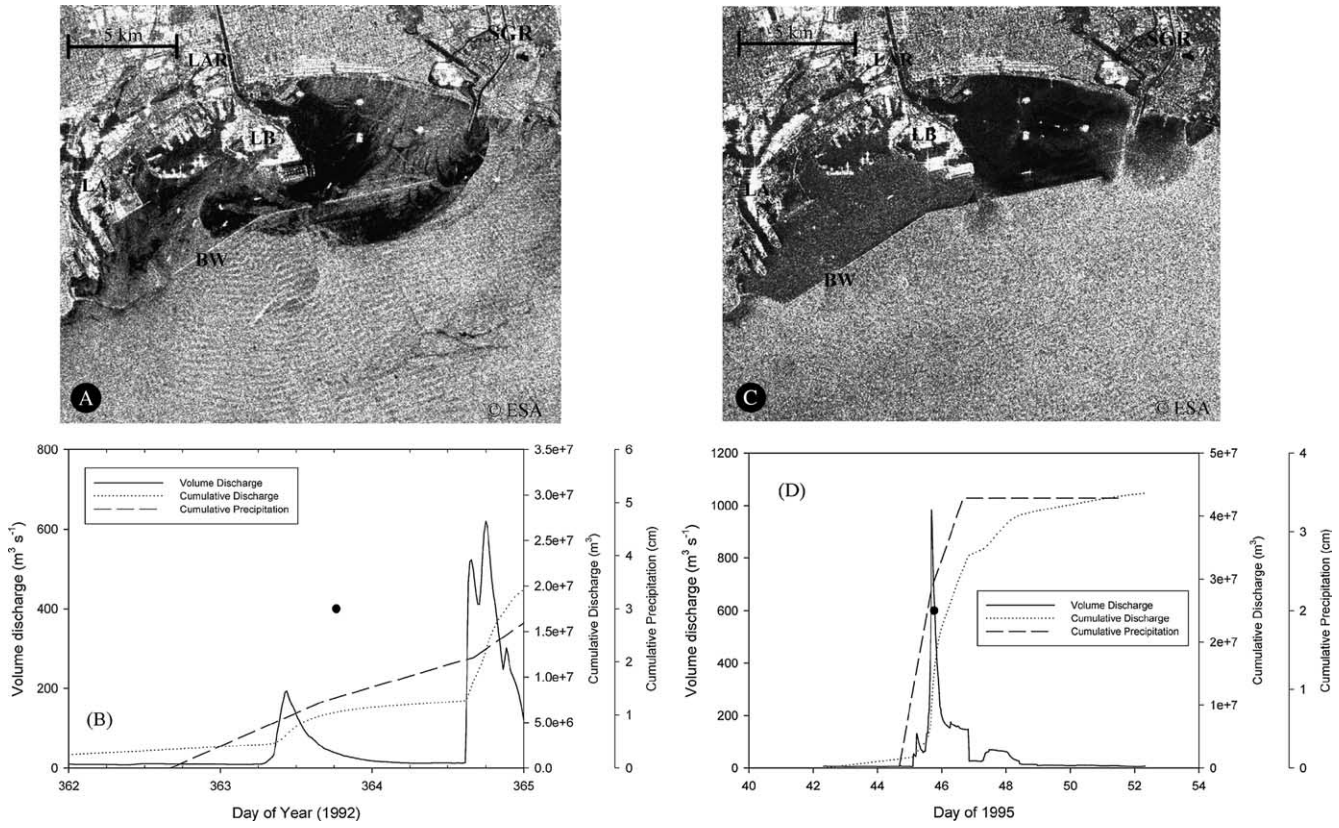

Fig. 3. Stormwater runoff plumes from the Los Angeles River (LAR) and San Gabriel River (SGR) in the Los Angeles (LA) and Long Beach (LB) Harbors, CA. The LA-LB Harbors breakwater is also indicated (BW). (A) ERS-1 SAR image on 28 December 1992 at 1835 GMT (12.5 m pixels). (B) Time series of Los Angeles River discharge rate (solid line), cumulative discharge volume (dotted line), and cumulative precipitation (dashed line). Dot shows time of SAR image of panel (A). (C) ERS-1 SAR image on for 14 February 1995 at 1833 GMT (12.5 pixels). (D) As panel B, but dot shows time of SAR image of panel C.

harbor resulted from the smaller rainfall (and runoff) event (Fig. 3A), whereas surfactants completely covered the eastern half of the LA-LB harbor area following a larger event (Fig. 3B).

3.2. Wastewater plumes

Treated municipal wastewater from urban areas of the Southern California Bight is commonly discharged into the coastal ocean through submerged sewage outfalls on the sea floor. Effluent is discharged into the ocean as a buoyant plume from an outfall diffuser, large diameter (3–4 m) pipes running approximately alongshore, typically located on the 60 m isobath. The diffusers comprise the final several hundred meters of pipe that are perforated on two sides with a series of ports whose diameters increase toward the end of the pipe. The diffusers are designed such that the sewage effluent forms a line source of buoyancy to promote rapid mixing with denser ambient ocean waters (Fischer et al., 1979; Wright et al., 1982; Roberts et al., 1989; Washburn et al., 1992). Under typical conditions of density stratification, the sewage effluent plume mixes with enough deep water to trap it at depth, often as deep as 30 m below the sea surface (e.g., Washburn et al., 1992; Wu et al., 1994; Dalkey and Shisko, 1996). Even though the effluent undergoes enhanced primary or secondary treatment, it still contains oils, grease, particles, metals, and, at times, chlorine (e.g., Raco-Rands and Steinberger, 2001). Trapping at depth prevents the effluent plume from reaching the surface and possibly interfering with human activities near shore such as swimming, fishing, and surfing. However, in winter when density stratification is reduced, the trapping may be ineffective allowing the sewage effluent to surface (e.g., Jones et al., 1990). When this happens the effluent may be rapidly transported to shore by wind and ocean surface currents.

Fig. 4A shows a RADARSAT SAR image from 24 December 1997 at 0148 GMT in which a dark, roughly diamond-shaped area appears over the Y-shaped diffuser of the city of Los Angeles' Hyperion sewage treatment plant. When this image was acquired the Hyperion plant was nominally discharging about $1.3 \times 10^6\,m^3\,day^{-1}$ ($350 \times 10^6\,gal\,day^{-1}$; Dorsey et al., 1995; Dalkey and Shisko, 1996). The diffuser from the Hyperion plant is located at the end of a 3.7 m diameter pipe

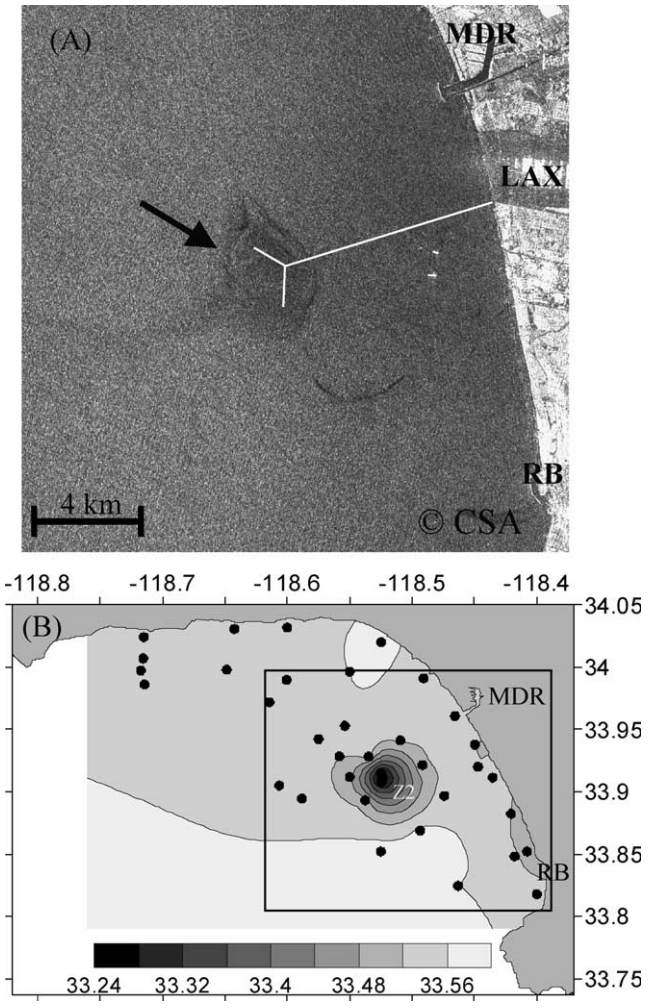

Fig. 4. (A) RADARSAT-1 SAR image on 24 December 1997 at 0147 GMT showing the surface signature of the municipal wastewater plume from the Hyperion outfall, off Los Angeles, CA (12.5 m pixels). Lines extending from shore indicate outfall location. Effluent is discharged through the Y-shaped diffuser at the end of the outfall. Also shown are Marina del Rey (MDR), the Los Angeles Airport (LAX), and Redondo Beach (RB). (B) Horizontal section of surface salinity on 20–21 December 1989 constructed from a grid of CTD stations (indicated by dots). Boxed region shows approximate area of the SAR image of A.

that extends about 8 km from shore and discharges on the 60 m isobath (Y-shaped lines, Fig. 4A). The dark region in Fig. 4A (see arrow) indicates lower backscatter compared with surrounding waters, consistent with smoothing of small surface waves due to surfactants from the surfacing Hyperion effluent plume. Turbulence within the plume may also smooth the surface and thus contribute to the low backscatter signature. The plume covers about 16 km^2 of the sea surface, extending approximately 1.5 km inshore of the diffuser. A narrow filament extending offshore from the plume suggests offshore advection. An interesting pattern of alternate black and white bands on scales of a few hundred meters on the northern boundary of the plume's surface signature may result from interactions of the spreading plume and near surface currents.

There were no coincident ship-based measurements when the SAR image in Fig. 4A was obtained to help verify that the plume had surfaced. However, an earlier study using CTD measurements demonstrated that the Hyperion plume periodically surfaces (Dalkey and Shisko, 1996). Fig. 4B illustrates such an occurrence for 21–22 December 1989 when a local minimum in sea surface salinity occurred over the diffuser during weak wintertime stratification (as was the case for Fig. 4A). The station right above the diffuser (Z2) also had lower temperature, lower dissolved oxygen, and higher suspended particulate loading compared with surrounding waters (data not shown). These results were consistent with a sewage plume signature. The coarse grid spacing of the CTD stations was adequate for detecting the plume, but SAR was more effective at resolving the horizontal scale of the plume and accurately assessing its spatial variability.

3.3. Natural hydrocarbon seeps

Clester et al. (1996) and Hornafius et al. (1999) estimate that natural hydrocarbon seeps offshore of Coal Oil Point, CA discharge 7800-8900 metric tons (54,000–62,000 barrels) per year of oil into the marine environment. Surface oil slicks from these seeps extending along the coast show up clearly as broad dark regions on SAR images such as in Fig. 5 from the northern Santa Barbara Channel. Smaller, sinuous dark regions away from the slicks in Fig. 5 may represent convergence zones where surfactants have accumulated. Prevailing currents over the Coal Oil Point seeps flow to the west (Harms and Winant, 1998; Dever et al., 1998; Winant et al., 2003), causing westward extension of the slicks away from their sources. The sources themselves occur in anticlines containing the oil-bearing Monterey formation (e.g., Quigley et al., 1999; Fischer, 1977; Allen et al., 1970) The isolation of natural seeps from other possible dark regions in SAR imagery, due to low winds primarily, can be determined through repeat imaging, because the seeps are consistently detected within a relatively small area.

Fig. 5A shows large oil slicks offshore of Coal Oil Point extending at least 50 km west of three source areas (indicated by arrows, Fig. 5A) on 10 December 1995. The slicks cover about 100 km^2 and, assuming a slick thickness in the range 0.01–0.1μ m (Macdonald et al., 1993), contain about 1–10 m^3 (about 6–60 barrels) of oil. Meanders in the slicks suggest the presence of complex flow structures on scales of a few km that distort the slicks as they advect westward. Fig. 5B, obtained 13 January 1996, shows an extreme example of this distortion in which a cyclonic (counterclockwise) eddy 10–15 km in diameter wraps the oil slicks

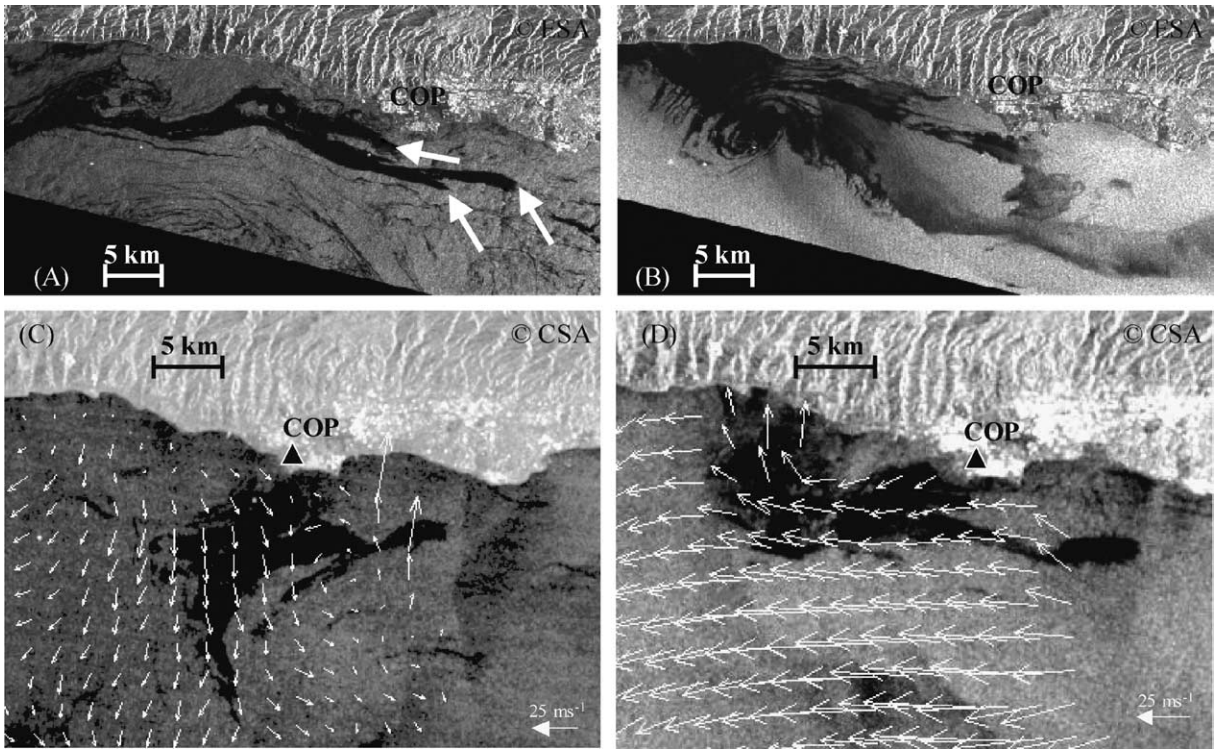

Fig. 5. Natural oil seeps off Coal Oil Point (COP), California. (A) ERS-2 SAR image on 10 December 1995 at 1840 GMT (100 m pixels). Arrows indicate three persistent hydrocarbon sources. (B) ERS-1 SAR image on 13 January 1996 at 1840 GMT (100 m pixels). (C) RADARSAT-1 SAR image on 10 February 1998 at 1400 GMT (100 m pixels). The triangle shows location of HF radar at COP. (D) RADARSAT-1 SAR image on 18 November 1998 at 1400 GMT (100 m pixels). Overlaid on (C) and (D) are current vectors from the HF radars, averaged over 12–24 h preceding SAR image acquisition.

into a spiral pattern 25 km west of Coal Oil Point. Harms and Winant (1998) and DiGiacomo and Holt (2001) report cyclonic eddies of comparable spatial scales in the Santa Barbara Channel. More recently, near shore anticyclonic eddies similar to that of Fig. 5B have been observed to change temperature and other water properties in depths of 10 m (unpublished observations from the Santa Barbara Channel Long Term Ecological Research project, see http://sbc.lternet.edu). The dark region northwest of the eddy in Fig. 5B may be a low wind region with little or no backscatter.

Oil slicks can be advected cross-shelf (onshore or offshore) depending on the current and wind fields near the coast. The SAR image of Fig. 5C shows oil slicks from the Coal Oil Point seep field being carried about 15 km offshore by surface currents on 10 February 1998. Current vectors (white arrows, Fig. 5C) are generally southward with flow speeds of about 0.15 ms^{-1} determined by two HF radars, one at Coal Oil Point (triangle, Fig. 5C and D) and another at Refugio Beach (just west of the area shown in Fig. 5C and D). Fig. 5D shows a contrasting example of onshore advection of oils slicks on 13 January 1996 in which a portion of the generally westward flow turns shoreward about 12 km west of Coal Oil Point. The presence of onshore flow and oil slicks within a few km of the coast suggests that these onshore flow events are a mechanism for transporting oil and tar closer to shore, which may lead to deposition on beaches in the region. The advection time for the oil to reach shore is less than 1.5 days assuming a 0.2 ms^{-1} flow speed from the HF radars and the ~25 km curving path of the oil from its sources to the coast based on the SAR image of Fig. 5D. Onshore wind transport is another likely, and perhaps more rapid, mechanism for transporting oil and tar to the coast.

The appearance of a small natural oil seep offshore of Redondo Beach (Fig. 6) illustrates the effect of wind speed on detection. A SAR image from 6 December 1995 at 1834 GMT shows a pair of small oil slicks from two adjacent sources as two dark regions (inside square, Fig. 6A). The wind speed was 1.3 ms^{-1} toward the west-southwest as recorded by a nearby weather buoy (NDBC 46045; position indicated by circle). A SAR image from the next day, 7 December 1995 at 1834 GMT, when the wind speed was 6.2 ms^{-1}, does not show the slicks, but rather an extensive, bright zone along shore indicating high backscatter. Under these conditions SAR is unable to distinguish surface roughness variations due to the oil seepage.

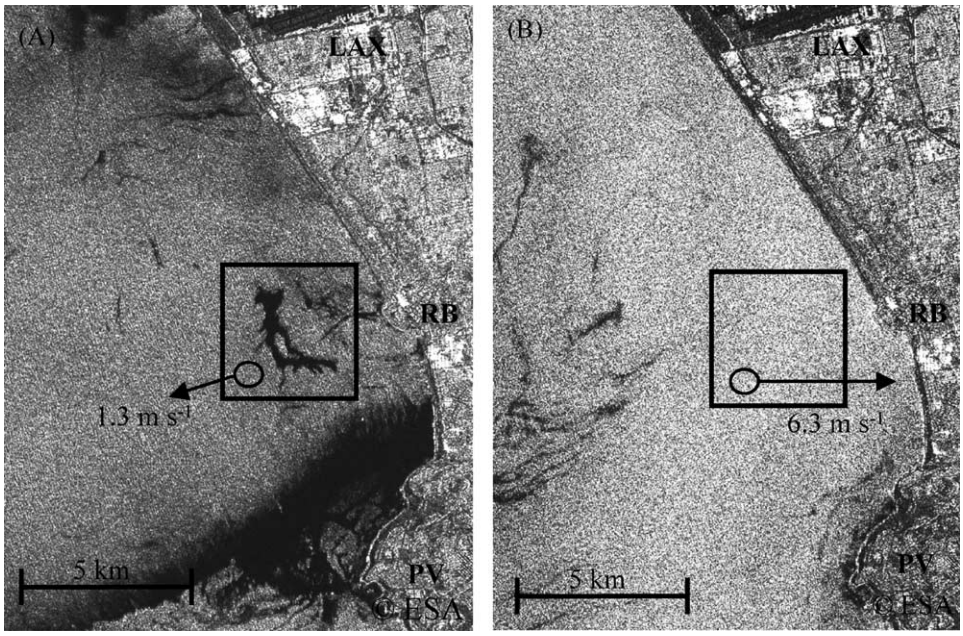

Fig. 6. Wind speed effects on SAR imaging of natural oil seeps off Redondo Beach, CA. (A) ERS-1 SAR image on 6 December 1995 at 1834 GMT (12.5 m pixels). Redondo Beach (RB), Los Angeles Airport (LAX), and Palos Verdes Peninsula (PV) are indicated. Buoy 46045 location is shown by circle. (B) As in (A) except ERS-2 SAR on 7 December 1995 at 1834 GMT (12.5 m pixels).

4. Discussion and conclusions

The Southern California Bight pollution hazards described here, i.e., stormwater plumes, wastewater plumes, and natural hydrocarbon seeps, were detectable in SAR imagery because they deposited surfactants on the sea surface that modulated surface roughness by smoothing capillary and small gravity waves. These surfactants varied by source. The Santa Monica Bay and Santa Barbara Channel seepage is natural in origin, consisting of petrogenic hydrocarbons originating from beneath the sea floor (Hornafius et al., 1999; Quigley et al., 1999). The stormwater plumes contain a broad suite of both natural terrigenous (e.g., plant detritus and soil particles) and anthropogenic (e.g., oils, grease) surface-active materials (Eganhouse et al., 1981; Tran et al., 1997). The surfactants in wastewater plumes are primarily anthropogenic (e.g., detergents, oils and human waste; Eganhouse and Kaplan, 1982a; Eganhouse and Kaplan, 1982b). Regardless of origin, the surfactants associated with these different hazard types produced areas of reduced backscatter (e.g., Fig. 2A) compared to the surrounding ocean, which were readily detected in the regional SAR imagery. The spatial scales and distributions of surfactants associated with these pollution hazards are the principal quantities derived from the SAR observations.

Based on the findings reported here, SAR appears well suited for characterizing runoff plume dynamics as a function of storm total precipitation, cumulative event discharge and timing of peak flow. The observations suggest a relationship between these parameters and surfactant loading. Furthermore, SAR is able to detect the varying distributions and residence times of surfactants within runoff plumes due to shoreline characteristics (e.g., open vs. semi-enclosed water bodies) and near shore properties (e.g., local currents). Harbors and ports may concentrate and retain runoff pollutants and pathogens given their limited exchange with the coastal ocean. This ability of SAR to detect and measure the spatial extent of stormwater plumes in both harbors and coastal waters under variable weather conditions should be valuable to coastal managers. Presently, the spatial extent and temporal evolution of these plumes is difficult to characterize adequately from ships due to cost, weather conditions, and the rapid evolution of the plumes under the influence of variable winds, currents, and freshwater discharge.

The surface expression of sewage plumes from subsurface ocean outfalls can also be detected in SAR imagery as shown here. Normally sewage plumes only surface in winter when ambient density stratification is weak (e.g., Fig. 4). However, for reasons that are not clear, outfall plumes occasionally breach the stratification and reach the surface during more stratified periods. Dalkey and Shisko (1996) report observations of the plume from the Hyperion treatment plant at the surface in SMB in September 1989, normally a month of strong stratification. September is also a month of heavy recreational beach use in southern California so the appearance of a sewage plume in surface waters is a potential concern for regional managers. Numerous

transport mechanisms exist, such as the small eddies in the region described by DiGiacomo and Holt (2001), which might rapidly move the effluent plume shoreward. Routine acquisitions of SAR imagery over outfall diffusers could reveal times when sewage plumes are on the sea surface which in turn would support managers charged with monitoring coastal water quality.

SAR imagery can be used to track oil in the coastal ocean such as might occur in an accidental oil spill. Complex spatial patterns of oil slicks from natural seeps in the SCB are frequently resolved in regional SAR imagery, such as the spiral pattern of the cyclonic eddy of Fig. 5B. Resolving this pattern from shipboard sampling would be extremely difficult due to its complexity, size, and episodic occurrence. Detecting these eddies is important because the residence times of oil near shore and its eventual fate may depend strongly upon whether or not dynamic features like this are present. Supplementing SAR observations with ground-based HF radar measurements is also promising, as sea surface currents derived from HF radar can account for spatial distributions of oil slicks (Figs. 5C and D). This pairing of SAR and HF radar merits further exploration given that HF radar coverage is rapidly increasing in US coastal waters as regional coastal ocean observing systems develop. Adequate resolution of the coastal wind field is also required. This might be provided ideally by an integrated network of buoys, satellite observations (SAR and scatterometry) and land-based stations.

A significant research issue that must be addressed is the nature and composition of the surfactants detected by SAR. The composition of oil slicks from natural hydrocarbon seepage and the grease and oils from sewage outfalls is fairly well understood. In contrast, the composition of surfactants in stormwater runoff is poorly understood, as are the connections between surfactants and distributions of toxic constituents and pathogens. If connections can be established, then SAR imagery might usefully predict the extent and duration of the negative effects due to stormwater plumes on beaches and near shore recreational waters. As part of this effort, detailed assessments are required to examine how surfactant composition and loading vary with watershed characteristics such as land use (e.g., urban, agricultural, mixed-use) and land cover (e.g., percent impervious surface).

SAR imagery has several advantages compared with other satellite approaches for use in marine pollution studies. We suggest that its use be broadened within the SCB, as has been done in Europe (e.g., Espedal et al., 1998; Gade and Alpers, 1999; Pavlakis et al., 2001). Among the advantages are its high spatial resolution (order 25–100 m), its sensitivity to the presence of surfactants as illustrated in this study, and its ability to obtain useful information regardless of cloud cover or darkness. The latter point is particularly relevant here given that stormwater discharge events occur during storms, when clouds often prevent observation by optical satellite sensors. The high spatial resolution of SAR imagery enables detection of small-scale hazards (e.g., Fig. 2C), as well as interactions between these hazards and small-scale ocean features such as eddies (e.g., Fig. 5B). The occurrence and interaction of these hazards and features would not be readily detected with most optical sensors. As an additional benefit, nearly all current and future SAR platforms include wide-swath coverage (>250 km) that improves the synoptic view of coastal regions.

Limitations of SAR include its inability to distinguish slicks from low wind or other low backscatter regions. At high wind speeds, SAR cannot detect slick signatures due to dispersion of surfactants (e.g., Fig. 6B). Also, it is not currently possible to confidently separate the various types of slicks discussed here using a single-frequency SAR, particularly at C-band (e.g., Gade et al., 1998). This could be improved by using dual frequencies, such as L- and X-bands (Gade et al., 1998). Another limitation of SAR is that it cannot determine the thickness of oil slicks, which is of particular importance for tracking oil spills (Fingas and Brown, 1997) and determining spill volumes. At present, however, the major limitations of SAR for detecting coastal pollution hazards are infrequent temporal coverage and restricted access to real-time and archived data. Improving temporal coverage to daily, for example, is only currently possible by using multiple SAR platforms (Holt and Hilland, 2000). Daily coverage would greatly enhance observation of evolving pollution threats such as stormwater plumes. It would also mitigate the effects of high and low winds by providing more observations of selected areas over a range of conditions. Improving data access, however, does not require new observing infrastructure, as currently Canada's RADARSAT and ESAs ERS-2 and Envisat SAR instruments are all operating nominally. In addition, RADARSAT-2 and Japan's ALOS mission carrying the PALSAR instrument are expected to launch soon. Much SAR data exists, but each international agency managing SAR programs has different scientific and programmatic objectives as well as inconsistent data access policies which complicate use and increase costs of data from multiple platforms. This severely limits use of existing SAR platforms and data sets as coastal management tools. Improved management of existing SAR programs could quickly remove these limitations.

Acknowledgment

We thank several people who contributed to this research. Leonard Davidian and Tirsit Kebede of the Los Angeles County Department of Public Works provided the river discharge and precipitation data. Brian

Emery of the University of California, Santa Barbara processed the HF radar data. John Oram of the University of California, Los Angeles supplied processed CTD data, acquired by the Environmental Monitoring Division of the City of Los Angeles's Bureau of Sanitation. The European Space Agency provided the ERS-1 and ERS-2 SAR imagery. The Alaska Satellite Facility provided the RADARSAT-1 SAR imagery. We also thank Ken Schiff and Steve Weisberg at the Southern California Coastal Water Research Project for valuable discussions. We also benefited from comments from anonymous reviewers. This research was supported by grants from NASA's Earth Science Enterprise program (JPL, UCSB, USC), the Minerals Management Service (UCSB), and the USC Sea Grant Program (USC). The JPL effort was supported by the National Aeronautics and Space Administration through a contract with the Jet Propulsion Laboratory, California Institute of Technology. Additional support was also provided by the David and Lucile Packard Foundation (UCSB). The Keck Foundation provided funding for the HF radars used in this research.

References

Allen, A.A., Schlueter, R.S., Mikolag, P.G., 1970. Natural oil seepage at Coal Oil Point, Santa Barbara, California. Science 170, 974–977.

Bay, S., Jones, B.H., Schiff, K.C., 1999. Study of the impact of stormwater discharge on Santa Monica Bay. Executive Summary Report prepared for the Los Angeles County Department of Public Works, Alhambra, CA. USC Sea Grant Program, Los Angeles, CA (USCSG-TR-02-99).

Clester, S.M., Hornafius, J.S., Scepan, J., Estes, J.L., 1996. Quantification of the relationship between natural gas seepage rates and surface oil volume in the Santa Barbara Channel (abstract). Eos. Trans., AGU 77(46), Fall Meeting Suppl., F419.

Culliton, T., Warren, M., Goodspeed, T., Remer, D., Blackwell, C., McDonough III, J., 1990. Fifty years of population changes along the nation's coasts, 1960–2010. Coastal Trends Series, Report No. 2, NOAA, Strategic Assessment Branch, Rockville, MD.

Dailey, M.D., Anderson, J.W., Reish, D.J., Gorsline, D.S., 1993. The California bight: background and setting. In: Dailey, M.D., Reish, D.J., Anderson, J.W. (Eds.), Ecology of the Southern California Bight: A Synthesis and Interpretation. University of California Press, Berkeley, CA, pp. 1–18.

Dalkey, A., Shisko, J.F., 1996. Observations of oceanic processes and water quality following seven years of CTD surveys in Santa Monica Bay. Bull. Southern California Acad. Sci. 95 (1), 17–32.

De Beukelaer, S.M., MacDonald, I.R., Guinnasso, N.L., Murray, J.A., 2003. Distinct side-scan sonar, RADARSAT SAR, and acoustic profiler signatures of gas and oil seeps on the Gulf of Mexico slope. Geo-Mar. Lett. 23 (3–4), 177–186.

Dever, E.P., Henderschott, M.C., Winant, C.D., 1998. Statistical aspects of surface drifter observations of circulation in the Santa Barbara Channel. J. Geophys. Res. 103 (C11), 24781–24797.

DiGiacomo, P.M., Holt, B., 2001. Satellite observations of small coastal ocean eddies in the Southern California Bight. J. Geophys. Res. 106 (C10), 22521–22544.

Dorman, C.E, 1982. Winds between San Diego and San Clemente Island. J. Geophys. Res. 87, 9636–9646.

Dorsey, J.H., Phillips, C.A., Dalkey, A., Roney, J.D., Deets, G.B., 1995. Changes in assemblages of infaunal organisms around wastewater outfalls in Santa Monica Bay, California. Bull. Southern California Acad. Sci. 94 (1), 46–64.

Eganhouse, R.P., Kaplan, I.R., 1982a. Extractable organic matter in municipal wastewaters. 1. Petroleum-hydrocarbons—temporal variations and mass emission rates to the ocean. Environ. Sci. Technol. 16 (3), 180–186.

Eganhouse, R.P., Kaplan, I.R., 1982b. Extractable organic matter in municipal wastewaters. 2. Hydrocarbons—molecular characterization. Environ. Sci. Technol. 16 (9), 541–551.

Eganhouse, R.P., Simoneit, B.R.T., Kaplan, I.R., 1981. Extractable organic matter in urban stormwater runoff. 2. Molecular characterization. Environ. Sci. Technol. 15 (3), 315–326.

Emery, B.M., Washburn, L., Harlan, J., 2004. Evaluating radial current measurements from CODAR high-frequency radars with moored current meters. Journal of Atmospheric and Oceanic Technology 21 (8), 1259–1271.

Espedal, H.A., Johannessen, O.M., 2000. Detection of oil spills near offshore installations using synthetic aperture radar (SAR). Int. J. Remote Sens. 21 (11), 2141–2144.

Espedal, H.A., Wahl, T., 1999. Satellite SAR oil spill detection using wind history information. Int. J. Remote Sens. 20 (1), 49–65.

Espedal, H.A., Johannessen, O.M., Johannessen, J.A., Dano, E., Lyzenga, D.R., Knulst, J.C., 1998. COASTWATCH'95: ERS 1/2 SAR detection of natural film on the ocean surface. J. Geophys. Res. 103, 24969–24982.

Espedal, H.A., Johannessen, O.M., Knulst, J., 1999. Satellite detection of natural films on the ocean surface. Geophys. Res. Lett. 23, 3151–3154.

Fingas, M.F., Brown, C.E., 1997. Review of oil spill remote sensing. Spill Sci. Technol. Bull. 4 (4), 199–208.

Fischer, P.J, 1977. Oil and tar seeps, Santa Barbara Basin, California, in California offshore gas, oil, and tar seeps: State of California. State Lands Commission Staff Report.

Fischer, H.B., List, E.J., Koh, R.C.Y, Imberger, J., Brooks, N.H., 1979. Mixing in Inland and Coastal Waters. Academic Press, New York.

Gade, M., Alpers, W., 1999. Using ERS-2 SAR images for routine observation of marine pollution in European coastal waters. Sci. Total Environ. 238, 441–448.

Gade, M., Alpers, W., Huhnerfuss, H., Masuko, H., Kobayashi, T., 1998. Imaging of biogenic and anthropogenic ocean surface films by the multifrequency/multipolarization SIR-C/X- SAR. J. Geophys. Res. 103 (C9), 18851–18866.

Gurgel, K.W, 1994. Shipborne measurements of surface current fields by HF radar. L'Onde Electrique 74 (5), 54–59.

Haile, R.J., Witte, J., Alamillo, J., Barrett, K., Cressy, R., Dermond, J., Ervin, C., Glasser, A., Harawa, N., Harmon, P., Harper, J., McGee, C., Millikan, R., Nides, M., 1996. An epidemiological study of possible adverse health effects of swimming in Santa Monica Bay. Monterey Park, CA, Report to the Santa Monica Bay Restoration Project.

Haile, R.J., Witte, J.S., Gold, M., Cressy, R., McGee, C.D., Millikan, R.C., Glasser, A., Harawa, N., Ervin, C., Harmon, P., Harper, J., Dermond, J., Alamillo, J., Barrett, K., Nides, M., Wang, G., 1999. The health effects of swimming in ocean water contaminated by storm drain runoff. J. Epidemiol. 104, 355–363.

Harms, S., Winant, C.D., 1998. Characteristic patterns of the circulation in the Santa Barbara Channel. J. Geophys. Res. 103 (C2), 3041–3065.

Hartman, B., Hammond, D., 1981. The use of carbon and sulfur isotopes as correlation parameters for the source identification of Beach Tar in the Southern-California Borderland. Geochim. Cosmochim. Acta 45 (3), 309–319.

Hickey, B.M., 1992. Circulation over the Santa Monica—San Pedro Basin and Shelf. Prog. Oceanogr. 30, 37–115.

Holt, B. 2004. SAR imaging of the ocean surface. In: Jackson, C.R., Apel, J.R. (Eds.), Synthetic Aperture Radar Marine User's Manual. NOAA NESDIS Office of Research and Applications, Washington DC, pp. 25–81.

Holt, B., Hilland, J., 2000. Rapid-repeat SAR imaging of the ocean surface: are daily observations possible? Johns Hopkins APL Tech. Digest 21 (1), 162–169.

Hornafius, J.S., Quigley, D.C., et al., 1999. The world's most spectacular marine hydrocarbon seeps (Coal Oil Point, Santa Barbara, California): quantification of emissions. J. Geophys. Res. 104 (C9), 20703–20711.

Jones, B., 2001. A comparison of visual observations of surface oil with Synthetic Aperture Radar imagery of the Sea Empress oil spill. Int. J. Remote Sens. 22 (9), 1619–1638.

Jones, B.H., Bratkovich, A., Dickey, T., Kleppel, G., Steele, A., Iturriaga, R., Haydock, I., 1990. Variability of physical, chemical and biological parameters in the vicinity of an ocean outfall plume. In: List, E.J., Jirka, G.H. (Eds.), Stratified Flows. American Society of Civil Engineers, New York, pp. 877–890.

Jones, B.H., Noble, M.A., Dickey, T.D., 2002. Hydrographic and particle distributions over the Palos Verdes Continental Shelf: spatial, seasonal and daily variability. Cont. Shelf Res. 22, 945–965.

Killus, J.P., Moore, G.E., 1991. Factor Analysis of hydrocarbon species in the South-Central Air Basin. J. Appl. Meteorol. 30, 733–743.

Lu, J., 2003. Marine oil spill detection, statistics and mapping with ERS SAR imagery in south- east Asia. Int. J. Remote Sens. 24 (15), 3013–3032.

Macdonald, I.R., Guinasso, N.L., et al, 1993. Natural oil-slicks in the Gulf-of-Mexico visible from space. J. Geophys. Res. 98 (C9), 16351–16364.

Munk, W.H., Armi, L., Fischer, K., Zachariasen, F., 2000. Spirals on the sea. Proc. R. Soc. London, Ser. A 456, 1217–1280.

National Research Council, 1990. Monitoring Southern California Coastal Waters. National Academy Press, Washington, DC.

National Research Council, 1993. Managing Wastewater in Coastal Urban Areas. National Academy Press, Washington, DC.

Noble, R.T., Weisberg, S.B., Leecaster, M.K., McGee, C.D., Dorsey, J.H., Vainik, P., Orozco-Bobon, V., 2003. Storm effects on regional beach water quality along the southern California shoreline. J. Water Health 1, 23–31.

Pavlakis, Tarchi, P.D., Sieber, A.J., 2001. On the monitoring of illicit vessel discharges using spaceborne SAR remote sensing—a reconnaissance study in the Mediterranean sea. Ann. Telecommun. 56 (11–12), 700–718.

Quigley, D.C., Hornafius, S.J., Luyendyk, B.P., Clark, J.F., Washburn, L., 1999. Decrease in natural marine hydrocarbon seepage near Coal Oil Point, California, associated with offshore oil production. Geology 27 (11), 1047–1050.

Raco-Rands, V.E., Steinberger, A., 2001. Characteristics of effluents from large municipal wastewater treatment facilities in 1997. In: Southern California Coastal Water Research. Project Annual Reports 1999–2000, pp. 28–44.

Roberts, P.J.W., Snyder, W.H., Baumgartner, D.J., 1989. Ocean outfalls. I: submerged wastefield formation. J. Hydraul. Eng. 115, 1–25.

Schiff, K.C., Allen, M.J., Zeng, E.Y., Bay, S.M., 2000. Southern California. Mar. Pollut. Bull. 41 (1–6), 76–93.

Solberg, A.H.S., Storvik, G., Solberg, R., Volden, E., 1999. Automatic detection of oil spills in ERS SAR images. IEEE Trans. Geosci. Remote Sens. 37 (4), 1916–1924.

Svejkovsky, J., Jones, B., 2001. Satellite imagery detects coastal stormwater and sewage runoff. Eos Trans. 82 (50), 621, 624, 625 and 630.

Tran, K., Yu, C.C., Zeng, E.Y., 1997. Organic pollutants in the coastal environment off San Diego, California. 2. Petrogenic and biogenic sources of aliphatic hydrocarbons. Environ. Toxicol. Chem. 16, 189–195.

Trivero, P., Fiscella, B., Gomez, F., Pavese, P., 1998. SAR detection and characterization of sea surface slicks. Int. J. Remote Sens. 19 (3), 543–548.

Wang, G.-Y., 1997. An Epidemiological Study of Possible Adverse Health Effects of Swimming in Santa Monica Bay. California and the World Ocean, San Diego. American Society of Civil Engineering, pp. 869–875.

Washburn, L., Jones, B.H., Bratkovich, A., Dickey, T.D., Chen, M.S., 1992. Mixing, dispersion, and resuspension in the vicinity of an ocean wastewater plume. J. Hydraul. Eng. 118 (1), 38–58.

Washburn, L., McClure, K.A., Jones, B.H., Bay, S.M., 2003. Spatial scales and evolution of stormwater plumes in Santa Monica Bay. Mar. Environ. Res. 56, 103–125.

Winant, C.D., Dever, E.P., Henderschott, M.C., 2003. Characteristic patterns of shelf circulation at the boundary between central and southern California. J. Geophys. Res. 108 (C2), 3021 doi:10.1029/2001JC001302.

Wismann, V., Gade, M., Alpers, W., Huhnerfuss, H., 1998. Radar signatures of marine mineral oil spills measured by an airborne multi-frequency radar. Int. J. Remote Sens. 19 (18), 3607–3623.

Wright, S.J., Wong, D.R., Zimmerman, K.E., Wallace, R.B., 1982. Outfall diffuser behavior in stratified ambient fluid. J. Hydraul. Div.-ASCE 108, 483–501.

Wu, Y.L., Washburn, L., Jones, B.H., 1994. Buoyant plume dispersion in a coastal environment: observations of plume structure and dynamics. Cont. Shelf Res. 14 (9), 1001–1023.